High-pressure phase transitions in BiMO_3 (M=Al, Ga, and In): *In situ* x-ray diffraction and Raman scattering experiments

Hitoshi Yusa*
Exploratory Nanomaterials Laboratory, National Institute for Materials Science, 1-1 Namiki, Tsukuba, Ibaraki 305-0044, Japan

Alexei A. Belik† and Eiji Takayama-Muromachi‡
International Center for Materials Nanoarchitechtonics, National Institute for Materials Science, 1-1 Namiki, Tsukuba, Ibaraki 305-0044, Japan

Naohisa Hirao§ and Yasuo Ohishi‖
Japan Synchrotron Radiation Research Institute, 1-1-1 Kouto, Sayo-cho, 679-5198 Hyogo, Japan
(Received 2 September 2009; revised manuscript received 30 October 2009; published 4 December 2009)

In situ x-ray diffraction and Raman scattering experiments using a diamond anvil cell revealed high-pressure forms of BiMO_3 (M=Al, Ga, and In) under hydrostatic conditions at room temperature. Various perovskite-type structures are found in each compound under pressure up to 11 GPa. However, none of the high-pressure forms was quenched at atmospheric pressure. All of the phase transitions are confirmed to be reversible. During decompression, symmetry changes, $R3m$ to $R3c$, $Cmcm$ to Cm, and $Pnma$ to $Pna2_1$ are observed in $BiAlO_3$, $BiGaO_3$, and $BiInO_3$ perovskite, respectively. Structure systematics of the BiMO_3 perovskites is given on the basis of the cationic size of M^{3+}.

DOI: 10.1103/PhysRevB.80.214103 PACS number(s): 61.50.Ks, 61.05.C−, 62.50.−p, 78.30.−j

I. INTRODUCTION

Lead zirconate titanate (PZT) is the most widely used ferroelectric material today. However, there is a growing need to replace this material with less environmentally damaging lead-free ferroelectrics. In particular, less toxic Bi-based perovskites are potentially attractive alternatives to PZT. The stereochemically active $6s^2$, lone pairs of the Bi^{3+} lead to large ferroelectric polarizations, as in the multiferroic $BiFeO_3$ perovskite (90 $\mu C/cm^2$) and $BiMnO_3$ perovskite.[1–5] Bi-based perovskites consisting of nonmagnetic elements, i.e., BiMO_3 (M=Al, Ga, In, and Sc), are also possible replacements for PZT.[6–13] Recently, perovskite structures of $BiAlO_3$ and $BiInO_3$ were recovered after a high $P-T$ treatment of their stoichiometric mixtures in a belt-type high-pressure apparatus.[8,9] The noncentrosymmetric rhombohedral perovskite structure ($R3c$) of $BiAlO_3$, predicted by *ab initio* calculations,[7] was confirmed by structure analysis.[8] In the case of $BiGaO_3$, a pyroxene-like structure ($Pcca$) rather than perovskite was recovered after a high $P-T$ treatment.[8] The theoretically predicted $BiGaO_3$ tetragonal perovskite with a large ferroelectric polarization exceeding that of $PbTiO_3$ has yet to be found experimentally.[7] $BiInO_3$ perovskite exhibits character as a polar crystal ($Pna2_1$). This sort of structure is very similar to the $GdFeO_3$-type perovskite structure ($Pnma$), except for the noncentrosymmetry.[9]

Crystal structure under pressure is never the same as one at ambient pressure. Indeed, a variety of pressure-induced reversible transformations were reported in ferroelectrics such as $PbTiO_3$ perovskite.[14–16] However, the high-pressure behavior of Bi-based perovskites has not been extensively investigated. Only a few studies have been done on multiferroics [e.g., $BiNiO_3$,[17] $BiMnO_3$,[18] and $BiFeO_3$ (Refs. 19–22)], in which complicated charge and orbital ordering in transition metals are linked to the structural phase transition. By replacing the magnetic elements in multiferroics with nonmagnetic elements, the role of Bi^{3+} can be identified without considering complicated magnetic behavior.

In this study, we elucidated the high-pressure behavior of BiMO_3 perovskites (M=Al, Ga, and In). *In situ* angle dispersive x-ray diffraction experiments under hydrostatic pressure enabled us to ascertain the crystal structures prior to decompression. Raman scattering experiments gave us complementary information for determining the structures. To the best of our knowledge, this is the first experimental study examining the high-pressure behavior of $BiAlO_3$, $BiGaO_3$, and $BiInO_3$ perovskites.

II. EXPERIMENTAL

$BiAlO_3$ and $BiInO_3$ perovskites, and $BiGaO_3$ pyroxene samples were prepared with a belt-type high-pressure apparatus from mixtures of Bi_2O_3, Al_2O_3, Ga_2O_3, and In_2O_3. In the case of $BiAlO_3$ and $BiGaO_3$, precursor mixtures of Al_2O_3 and $Bi_{25}AlO_{39}$ for $BiAlO_3$ and $Bi_2Ga_4O_9$ and $Bi_{25}GaO_{39}$ for $BiGaO_3$ were synthesized before the high-pressure treatment by heating them at 1023 K under ambient pressure for 8 h. The stoichiometric mixtures were enclosed in Au capsules and compressed at 6 GPa, and the mixture for $BiAlO_3$ was heated at 1273 K for 40 min, while the one for $BiGaO_3$ was heated at 1473 K for 15 min. The high-pressure synthesis of the $BiInO_3$ perovskite samples used a mixture of Bi_2O_3 and In_2O_3 that had been dried at 873 K for 8h. The sample in the Au capsule was heated at 1273 K under 6 GPa for 80 min. The details of the synthesis and characterization of these samples are described elsewhere.[8,9]

A symmetrical diamond anvil cell (DAC) with a culet diameter of 0.4 mm was used in the *in situ* x-ray and Raman scattering experiments. Prior to the x-ray experiments, the samples were pulverized by using a mortar or a vibratory

ball mill. The powder sample was placed in the chamber (0.15 mm diam) of a rhenium gasket (0.1 mm thick) seated on the diamond anvil. A few small grains of ruby (less than 5 microns) were also put in the sample chamber to measure the pressure by ruby fluorescence.[23] The sample chamber was filled with a pressure medium (methanol: ethanol: water =16:3:1) that would give a hydrostatic condition. The high-pressure x-ray powder diffraction experiments were performed on the BL04B2 and BL10XU beam lines at SPring-8. Monochromatic x-rays (38 or 30 keV) were focused and collimated to less than 50 micrometers in diameter on the sample in the DAC. Diffracted x-rays were detected by using a 300-mm-square (100 micrometers/pixel) imaging plate (IP) placed at a distance of 487.723 mm from the sample. If necessary, to resolve overlapping Debye rings, the separation between the IP and the sample was lengthened to 687.723 mm and the high-resolution readout mode of the IP (50 micrometers/pixel) was utilized. We collected diffraction patterns at room temperature at intervals of 1–3 GPa in compression up to 10.5 GPa and in decompression to examine the hysteresis of the phase transition. The high-intensity x-rays from the synchrotron radiation enabled one diffraction pattern to be taken within 10 minutes. A computer program (FIT2D) (Ref. 24) was used to convert the Debye rings into one-dimensional x-ray profiles (2θ vs intensity). The x-ray profiles were analyzed with the Rietveld and LeBail methods of the GSAS (Ref. 25) and RIETAN-2000 programs.[26] The details of the high-pressure x-ray experiments, including the data treatments, are described elsewhere (e.g., Ref. 27)

Unpolarized Raman spectra of the powdered samples at high pressure were collected at room temperature with a Raman spectrometer (NR-1800, Jasco) equipped with a single monochromator (1800 grooves/mm) and a liquid-nitrogen-cooled charge coupled device (CCD) detector. The Raman spectrum was induced by an Ar^+ laser (514.5 nm) beam focused to about 3 micrometers in diameter on the sample in the DAC. We took great care not to apply too much laser power. A Raman-inactive argon pressure medium was used. The pressure in the Raman scattering experiments was determined with the ruby fluorescence method.[23]

III. RESULTS AND DISCUSSION

A. High-pressure phase transitions in $BiAlO_3$ perovskite

Fig. 1 shows typical x-ray profiles at different pressures. The splitting peaks exhibit a deviation from what would be expected for an ideal cubic perovskite structure. There are several peak splitting schemes for a perovskite structure.[28] In particular, the first and fourth peaks (corresponding to 100_{pc} and 200_{pc} reflections in pseudocubic perovskite, hereafter, *pc* denotes a pseudocubic setting) should not be split in the diffraction profile of rhombohedral perovskites. On the other hand, the 111_{pc} peak should not be split in the profile of tetragonal perovskites. The profiles up to about 3 GPa clearly exhibit rhombohedral-type ($R3c$) peak splitting. The splitting gradually coalesces into a single peak with increasing pressure to about 7 GPa; thus, at first, we expected a rhombohedral ($R3c$) to the ideal cubic ($Pm\bar{3}m$) phase transition for

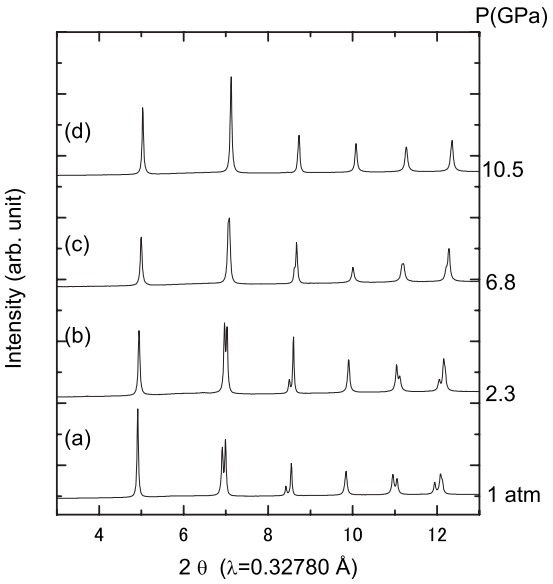

FIG. 1. Representative x-ray diffraction profiles from $BiAlO_3$ samples (a) at ambient pressure, (b) at 2.3, (c) 6.9, and (d) 10.5 GPa under hydrostatic conditions. Monochromatic x-ray radiation of 38 keV was used.

$BiAlO_3$ perovskite. However, as shown in Fig. 2, distinct Raman modes existed even above 10 GPa. Therefore, the above transition sequence is excluded because $Pm\bar{3}m$ perovskite never exhibits the first-order Raman active mode. We can see the characteristic feature in the lower wavenumbers [Fig. 2(a)], where the peak at the lowest wavenumber gradually separates with increasing pressure, and the higher peak moves toward the next peak and eventually coalesces into the peak at about 4 GPa. Moreover, the so-called "soft" mode around 121 cm^{-1} shifts toward lower wavenumber with increasing pressure [Fig. 2(b)]. We examined the spectral similarity between $BiAlO_3$ and other aluminate perovskites to identify the soft mode. In $LaAlO_3$ perovskite, which is one of the most studied aluminate perovskites, the high-pressure phase transition from rhombohedral ($R\bar{3}c$) to cubic perovskite ($Pm\bar{3}m$) is induced by the rotation of the AlO_6 octahedra around the hexagonal [001] direction.[29–32] Accordingly, the corresponding A_{1g} mode around 123 cm^{-1} shifts to lower wavenumbers with increasing pressure until the cubic phase appears.[31] In the present $BiAlO_3$ perovskite as well, the soft mode (A_{1g} for $R\bar{3}c$ should be reassigned to A_1 for $R3c$) occurred at 121 cm^{-1}. Therefore, the transition occurring at 4 GPa would likely be correlated with the AlO_6 octahedral rotation. Considering the constraints imposed by the peak splitting of the x-ray profiles together with the above-mentioned changes in the Raman spectra, we expected that the transition phase would keep rhombohedral symmetry. We checked the number of Raman active modes, which enumerate the possible rhombohedral perovskites, such as $R3c$, $R\bar{3}c$, $R\bar{3}m$, and $R3m$. According to factor group analysis,[33] $R3c$, $R\bar{3}c$, $R\bar{3}m$, and $R3m$ perovskites, respectively, have 13 ($4A_1+9E$) modes, 5 ($A_{1g}+4E_g$) modes, 7 ($3A_{1g}+4E_g$) modes, and 9 ($4A_1+5E$) modes for Raman active. As shown

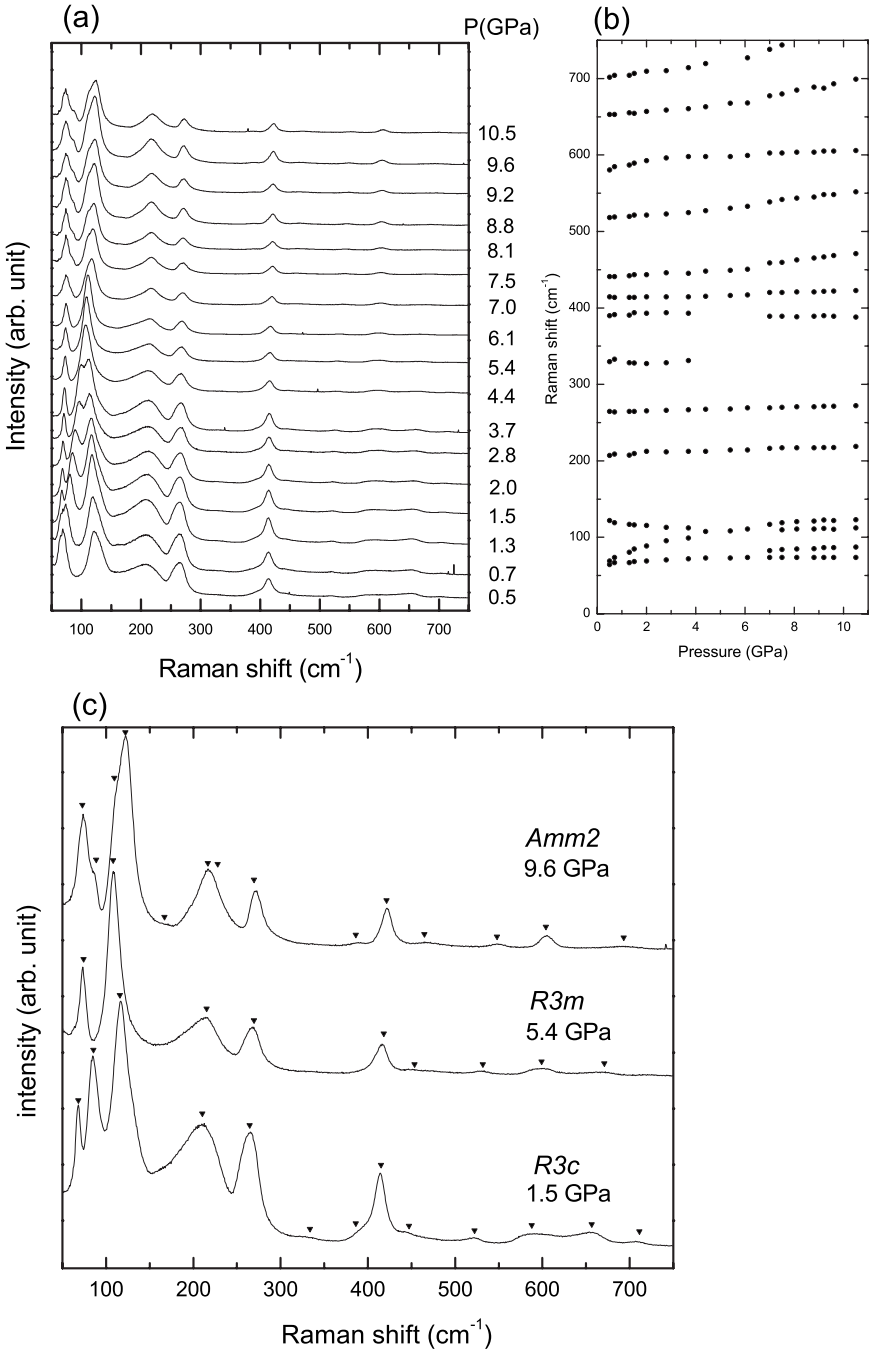

FIG. 2. (a) Variation in unpolarized Raman spectra from $BiAlO_3$ samples with pressure under quasihydrostatic compression. (b) Pressure dependence of the observed Raman modes in $BiAlO_3$. (c) Representative Raman spectra for each phase in $BiAlO_3$. The marks indicate the position of the Raman modes.

in Fig. 2(c), we observed nine modes at 5.4 GPa. Therefore, we concluded that the most probable symmetry would be $R3m$. The rotation scheme of AlO_6 in the transition from $R3c$ to $R3m$ is schematically shown in Fig. 3. When we measured Raman spectra, we could not see any hysteresis with pressure in this transition. Moreover, considering the continuous volume change in the transition pressure (Fig. 4), the second-order transition would be expected. The bulk modulus (B_0) was determined to be 121 ± 11 GPa by fitting the $P-V$ data in the rhombohedral phase ($R3c$) to the Birch-Murnaghan equation of state (B-M EoS) with $B_0'=4$. Theoretical studies on the hypothetical ideal cubic perovskite structure in $BiAlO_3$ give the bulk moduli and their pressure derivatives of 188–219 GPa and 4.27–5.15, respectively.[11,12] The large discrepancy in bulk moduli suggests that the theoretical calculation does not account for the AlO_6 rotations.

The Raman spectra show that the second transition begins around 7 GPa. An additional peak emerges at the shoulder of the 100_{pc} peak, and the 111_{pc} peak gradually splits with increasing pressure. At least 13 Raman modes were observed after this transition. Judging from the number of Raman active modes, rhombohedral structures are not applicable to the

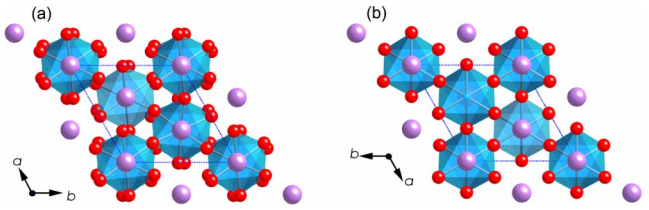

FIG. 3. (Color online) Crystal structures of (a) *R*3*c* and (b) *R*3*m* perovskites along the *c* axis in $BiAlO_3$. Small spheres and large spheres are oxygen and bismuth, respectively. Polyhedra indicate AlO_6 octahedra.

third phase. To examine the structural properties of the third phase, the splitting of the x-ray peaks was studied again by using a high-resolution configuration for the IP. We found that the 200_{pc} peak clearly splits in the diffraction profiles (Fig. 5). Therefore, we eliminated the tetragonal phase from the possible structures. Next, we checked the number of Raman active modes for common orthorhombic perovskites belonging to the *Pnma*, *Cmcm*, and *Amm*2 space groups. Although the 24 Raman modes predicted for *Pnma* ($7A_g+5B_{1g}+7B_{2g}+5B_{3g}$) and *Cmcm* ($7A_g+7B_{1g}+4B_{2g}+6B_{3g}$) perovskites would seem to include the 13 observed modes. However, considering a slight change in Raman spectra feature, a sudden increase in number of Raman modes could not be plausible. Consequently, we assumed that the *Amm*2 perovskite possessing 15 ($6A_1+A_2+4B_1+5B_2$) modes is the most probable structure among orthorhombic perovskites. Moreover, this phase transition sequence from *R*3*m* to *Amm*2 where the *B* site cations move off the center of the octahedral is known to occur in $BaTiO_3$ perovskites at low temperature.[34] We did not detect a significant change in volume at this transition (Fig. 4). This is also consistent with the small volume change (less than 1%) observed in $BaTiO_3$. Although the ambient structure of $BiAlO_3$ exhibits isotypic structure with the multiferroic $BiFeO_3$, at least up to 10 GPa, different structural evolutions are confirmed.[22]

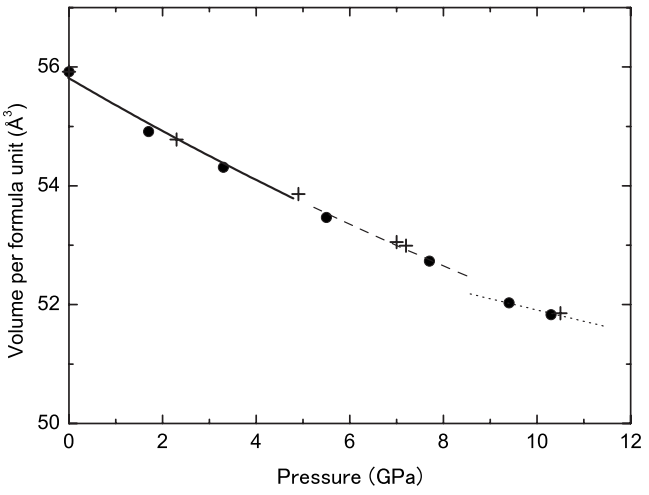

FIG. 4. Compression curve and pressure-volume data of $BiAlO_3$. Solid circles and crosses represent data from the first and second experiment, respectively. All volume data are normalized per formula unit. The compression curve was obtained by fitting the volume data until 5 GPa to the Birch-Murnaghan equation of state.

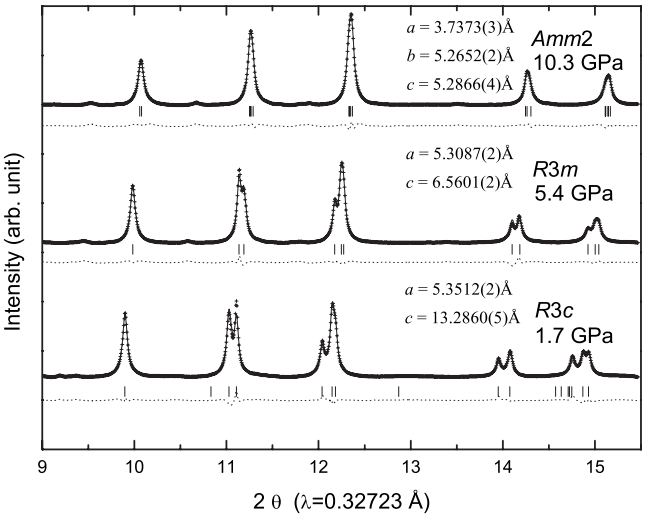

FIG. 5. X-ray profile deconvolution of perovskite phases in $BiAlO_3$ by using LeBail method of the RIETAN2000 program (Ref. 26). The difference (dotted line) between the observed (crosses) and fitted pattern (thin line) is shown on the same scale. Vertical bars represent the calculated positions of diffraction peaks of the perovskite phases. Monochromatic x-ray radiation of 38 keV was used.

B. High-pressure phase transitions in $BiGaO_3$

The x-ray diffraction profiles changed significantly twice during compression, at 3.2 and 6.3 GPa [Fig. 6(a)]. At 3.2 GPa, there was a mixture of the ambient phase (*Pcca*) and a high-pressure phase (Fig. 7). During decompression [Fig. 6(b)], the phase transition exhibits a large hysteresis, in which the high-pressure phase remains even near ambient pressure. If we look carefully at the profile after decompression, a trace of the high-pressure phase can be still recognized. The transition properties can also be seen in Raman spectra (Fig. 8). The high-pressure phase is identical to the previously reported monoclinic perovskite (*Cm*) stabilizing in the solid solution of $BiGaO_3$-$BiAlO_3$ join at ambient pressure.[8] The volume change in the phase transition from *Pcca* pyroxene to *Cm* perovskite was calculated to be 6.5% from the x-ray profile showing the two coexisting phases at 3.2 GPa (Fig. 7). The compression curves determined from the bulk modulus by fitting the $P-V$ data to B-M EoS are shown in Fig. 9. Due to metastability, the ambient pressure volume of *Cm* perovskite (V_0=64.86 Å^3) is slightly different from the value extrapolated from the compression curve (V_0=64.41 Å^3). The bulk moduli of *Pcca* pyroxene and *Cm* perovskite were calculated to be 79 ± 2 GPa and 84 ± 3 GPa with B_0'=4. In contrast to the expected large bulk modulus (179–218 GPa) given by *ab initio* calculations[11,12] for cubic $BiGaO_3$ perovskite, the present result exhibits a significantly small value.

The previous report[8] indicated that the solid solution of Al^{3+} into $BiGaO_3$ stabilizes *Cm* perovskite at ambient pressure. According to the present study, pressure makes the *Cm* perovskite stabilize even in $BiGaO_3$. This suggests that both pressure and compositional changes yield the same effects upon crystallizing the *Cm* perovskites. We plotted the zero pressure volume of $BiAl_{0.75}Ga_{0.25}O_3$ perovskite on Fig. 9 to

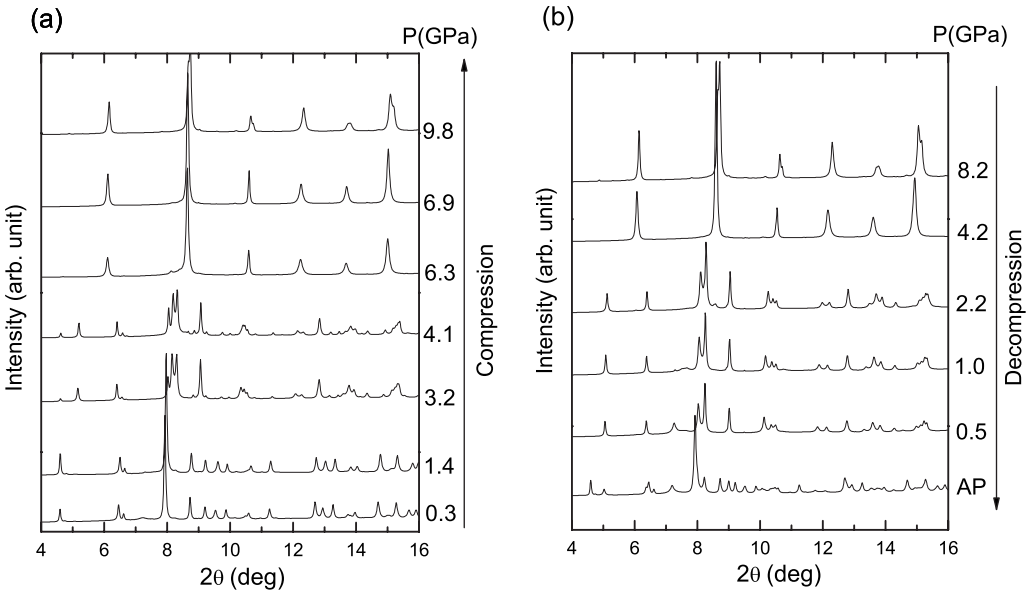

FIG. 6. X-ray profiles from $BiGaO_3$ sample. (a) Compression. (b) Decompression. Monochromatic x-ray radiation of 30 keV was used.

compare with the high-pressure volume of $BiGaO_3$ perovskite. The plot shows that the replacement of Ga^{3+} by Al^{3+} in the crystal structure makes the volume close to the compressed state.

As described in Ref. 8, the *Cm* perovskite is structurally similar to tetragonal $PbVO_3$ perovskite (space group *P*4*mm*),[35,36] which is isotypic structure with $PbTiO_3$. *Ab initio* calculations predicted that a possible *P*4*mm* $BiGaO_3$ perovskite exhibits a larger spontaneous polarization than $PbTiO_3$.[7] However, the *P*4*mm* perovskite did not appear in $BiGaO_3$; instead, the *Cm* perovskite appeared at high pressure.

The second high-pressure phase that emerges at 6.3 GPa on the x-ray profile (Fig. 6) is apparently similar to cubic perovskite. However, since the Raman peaks appeared at every pressure (Fig. 8), the structure could not be the ideal cubic perovskite phase ($Pm\bar{3}m$). If we look carefully at the full width at half maximum (FWHM) of the x-ray peaks, we can see broadening due to splitting at all peaks except the 111_{pc} peak. Therefore, the structure seems to be tetragonal or orthorhombic rather than rhombohedral. The large changes with pressure and large hysteresis in the Raman spectra imply a first-order transition. At least 13 Raman modes are associated with this phase (Fig. 8). Let us examine the number of Raman active modes of possible phases derived from the factor analysis. The common tetragonal perovskite phases, *P*4*mm*, *P*4/*mbm*, and *I*4/*mcm*, exhibiting 10 ($4A_1+B_1+5E$), 4 ($A_{1g}+B_{1g}+B_{2g}+E_g$), and 7 ($A_{1g}+B_{1g}+2B_{2g}+3E$) modes, respectively, could not account for the observed number of modes. On the other hand, 24 modes in the orthorhombic *Pnma* ($7A_g+5B_{1g}+7B_{2g}+5B_{3g}$) and *Cmcm* ($7A_g+7B_{1g}+4B_{2g}+6B_{3g}$) perovskites can account for the number of observed modes. Moreover, the 111_{pc} peak of *Cmcm* perovskite does not split, which is consistent with the observed diffraction pattern (Fig. 10). Therefore, we believe that *Cmcm* perovskite is the most probable choice to explain the properties of the high-pressure phase. The noncentrosymmetric (*Cm*) to centrosymmetric (*Cmcm*) structural evolution accompanying the shift in the Bi cation and the tilt of the GaO_6 octahedron could be responsible for the volume change ($\Delta V=5.0\%$) at this transition.

Another phase transition occurred during compression at 9.8 GPa in the x-ray diffraction pattern and at 9.7 GPa in the Raman spectrum. The 111_{pc} peak in the x-ray profile clearly splits, as do the other peaks. Judging from the feature of main peaks, at first, $GdFeO_3$-type (*Pnma*) phase was

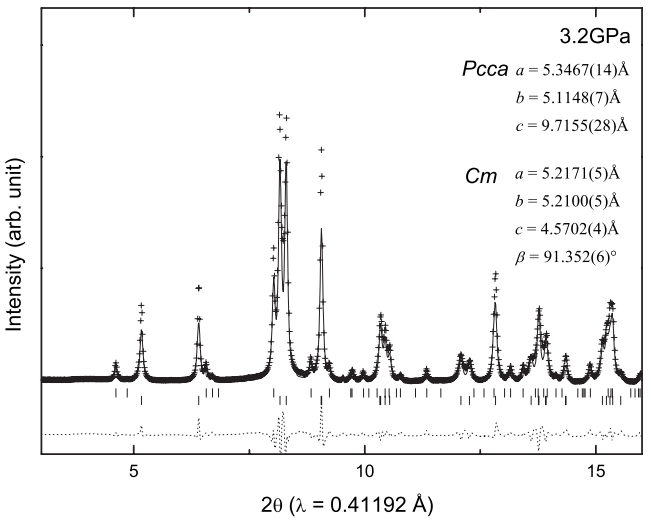

FIG. 7. Multiple phase analysis using GSAS for the mixture phase of *Pcca* pyroxene and *Cm* perovskite in $BiGaO_3$ at 3.2 GPa. The difference (dotted line) between the observed (crosses) and fitted pattern (thin line) is also shown on the same scale. Vertical bars represent the calculated positions of diffraction peaks; top, pyroxene; bottom, *Cm* perovskite. Monochromatic x-ray radiation of 30 keV was used.

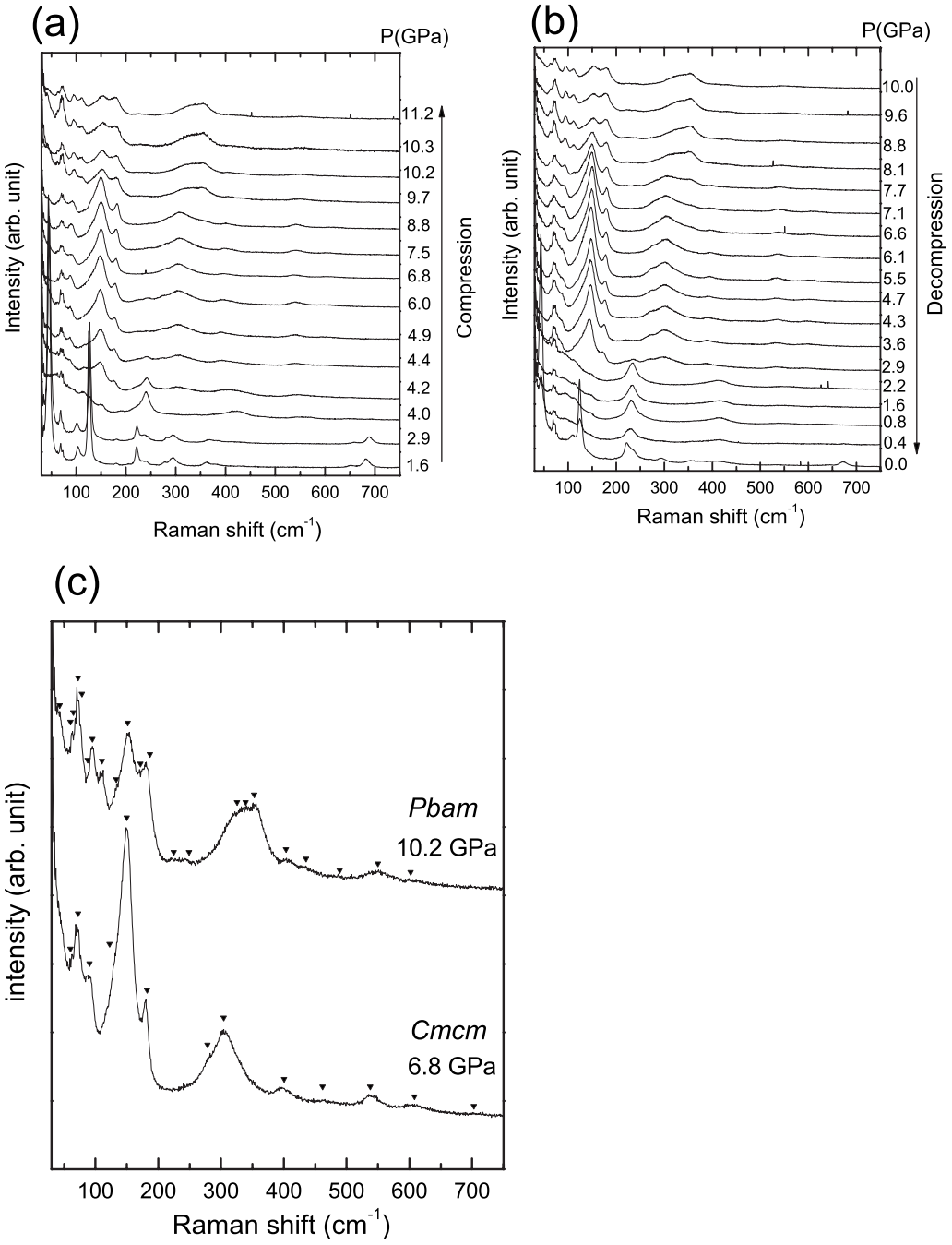

FIG. 8. Variation in unpolarized Raman spectra from $BiGaO_3$ samples with pressure under quasihydrostatic compression. (a) Compression. (b) Decompression. (c) Representative Raman spectra for orhthorhombic perovskite phases in $BiGaO_3$. The marks indicate the positions of Raman modes.

assumed, because the phase sequence from *Cmcm* to *Pnma* occurs during high-temperature phase transitions in ABO_3 perovskites such as $NaTaO_3$,[37] and $SrHfO_3$.[38] However, a typical reflection 111, which commonly appears in *Pnma* perovskite, was not observed in the present profile. Furthermore, we take particular note of additional weak peaks emerging around 4.8°, 5.3°, and 5.75°. A superstructure was considered to index all peaks including these additional peaks. The fitting analysis suggests that the phase is probably $PbZrO_3$-type (*Pbam*) perovskite (Fig. 10).[39] Although the transition does not involve changing the number of formula unit in the unit cell, the axes' relations change as follows, ($a_{Pbam} \sim (1/\sqrt{2}) a_{Cmcm} \sim \sqrt{2} a_{Pm3m}$; $b_{Pbam} \sim \sqrt{2} b_{Cmcm} \sim 2\sqrt{2} a_{Pm3m}$; $c_{Pbam} \sim c_{Cmcm} \sim 2 a_{Pm3m}$). After the transition, the number of Raman active modes significantly increased to 60 ($16A_g + 16B_{1g} + 14B_{2g} + 14B_{3g}$). In fact, in addition to the appearance of new peaks around 110 cm^{-1} at 10.2 GPa, we can see that the broadening of a band located around 320 cm^{-1} clearly exhibits the splitting of modes [Fig. 8(c)]. Therefore, we believe that the large changes in the Raman spectra reflect not only changes in the tilting and distortion schemes of GaO_6 octahedra but also the shifts in Bi^{3+} atoms.

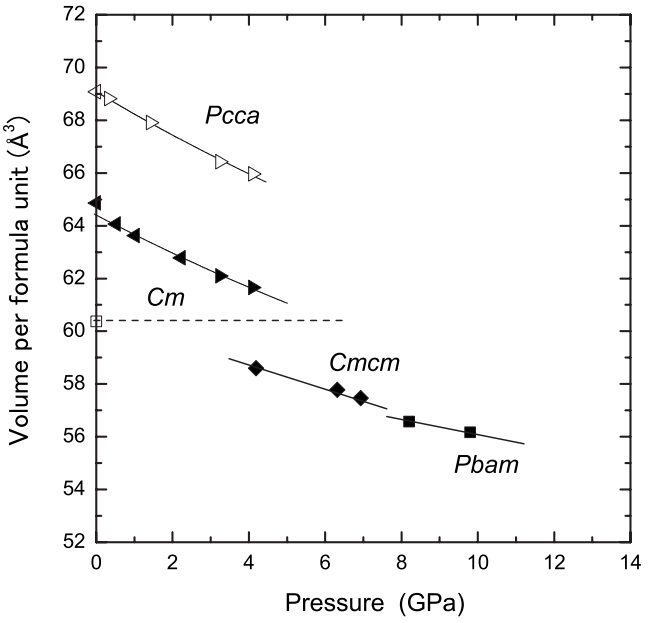

FIG. 9. Compression curves and pressure-volume data of $BiGaO_3$. Open triangles, solid triangles, diamonds, and squares represent *Pcca* pyroxene, *Cm*, *Cmcm*, and *Pbam* perovskites, respectively. Right and left pointing triangles mean compression and decompression, respectively. An open square represents the ambient volume of *Cm* perovskite in $BiAl_{0.75}Ga_{0.25}O_3$ (Ref. 8). All volume data are normalized per formula unit. The compression curves of pyroxene and *Cm* perovskite were obtained by fitting the volume data to the Birch-Murnaghan equation of state. The *Cmcm* and *Pbam* perovskite data are fitted by linear functions.

C. High-pressure phase transitions in $BiInO_3$

As previously reported,[9] the starting $BiInO_3$ perovskite is slightly distorted from the *Pnma* structure of most

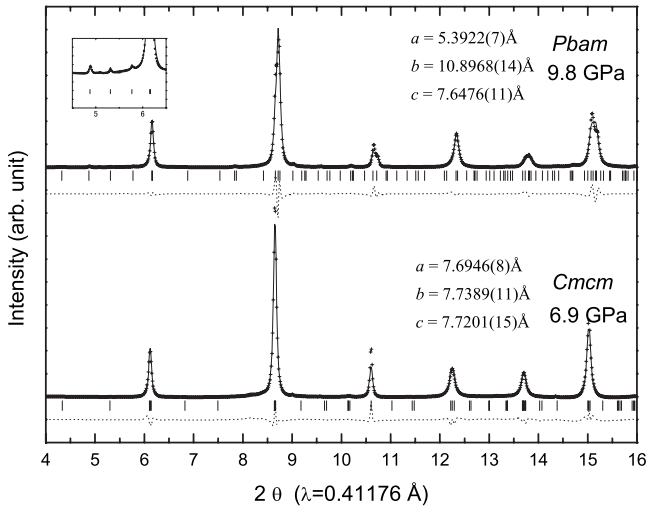

FIG. 10. X-ray profile deconvolution of orthorhombic perovskite phases in $BiGaO_3$ by using LeBail method of the RIETAN2000 program (Ref. 26). The difference (dotted line) between the observed (crosses) and fitted pattern (thin line) is also shown on the same scale. Vertical bars represent the calculated positions of diffraction peaks of the perovskite phases. Monochromatic x-ray radiation of 30 keV was used.

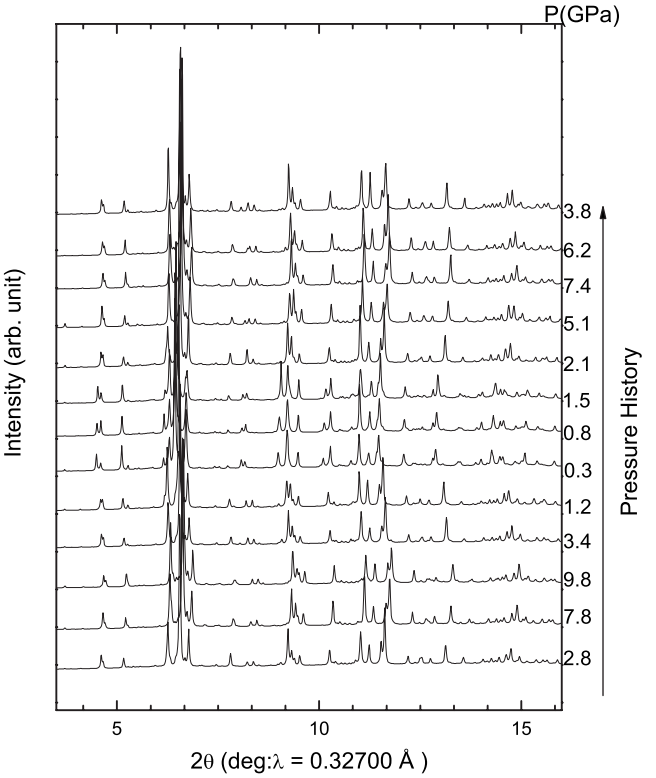

FIG. 11. X-ray profiles from $BiInO_3$ sample. History of pressure is indicated by the right axis. Monochromatic x-ray radiation of 38 keV was used.

$GdFeO_3$-type perovskites. The x-ray diffraction patterns indicated that the transition occurs before 2.8 GPa (Fig. 11). No further structural change occurred upon further compression to 9.8 GPa. The high-pressure phase reverts to the starting phase at 0.3 GPa during decompression. The recompression experiment reproduced the high-pressure phase at 2.1 GPa.

The high-pressure phase has a diffraction pattern that is similar to that of the ambient $Pna2_1$ perovskite phase. Therefore, we used the Rietveld method to analyze the diffraction profile, while assuming the same extinction rules as in the $Pna2_1$ perovskite.[40] As indicated in the refinement result (Fig. 12), the *Pnma* structure is appropriate for the high-pressure phase. A volume jump (ΔV=1.9%) at the transition pressure clearly shows that the structural change from $Pna2_1$ to *Pnma* is a first-order transition [Fig. 13(a)]. The $Pna2_1$ phase has a polar structure stemming from a large displacement of Bi^{3+} from the mirror plane of *Pnma*, as reported in the previous paper, where Bi^{3+} is away from the centroids of their oxygen coordination because of the strongly distorted oxygen environment caused by the lone electron pair of Bi^{3+}. Namely, at the transition pressure, Bi^{3+} promptly moves parallel to the *c* axis in the $Pna2_1$ structure and settles on the mirror plane in *Pnma* (Fig. 14). In lattice parameters with pressure [Fig. 13(b)], we observed a jump between *c* axis in $Pna2_1$ and *b* axis in *Pnma*, which is responsible for the displacement of Bi^{3+} at the transition. By fitting the $P-V$ data of the *Pnma* structure to B-M EoS, the bulk modulus (B_0) was calculated to be 152 ± 2 GPa with B_0'=4. This value is in good agreement with the theoretical one (B_0

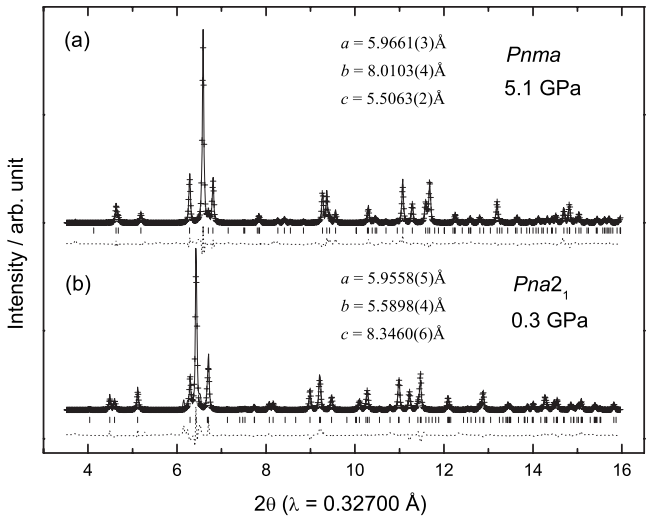

FIG. 12. Powder x-ray diffraction profiles of (a) *Pnma* and (b) $Pna2_1$ perovskites in $BiInO_3$, as obtained by the Rietveld method (GSAS). The observed profiles (crosses) are the same as those in Fig. 11. The difference (dotted line) between the observed and fitted pattern (thin line) is shown on the same scale. For the *Pnma* perovskite, atomic coordinates are Bi(4*c*) [0.0472(5), 0.25, 0.9851(10)], In(4*a*) (0.5,0,0), O1(4*c*) [0.476(10), 0.25, 0.232(8)], and O2(8*d*) [0.313(5), 0.018(6), 0.618(5)]. For the $Pna2_1$ perovskite, the same atomic coordinates at atmospheric pressure in Ref. 9 are assumed. Background has been subtracted. (a) R_{wp}=8.6%, (b) R_{wp}=6.4%.

=158 GPa with B_0'=4.15) obtained from *ab initio* calculations for cubic $BiInO_3$ perovskite.[12] The *Pnma* perovskite of $BiInO_3$ stabilizes at about 2 GPa. The pressure is comparable to the transition pressures from *C*2/c to *Pnma* phase in $BiCrO_3$, $BiScO_3$, and $BiMnO_3$.[18] On the other hand, in the $BiFeO_3$ perovskites, the *Pnma* phase appears above 10 GPa.[21]

$GdFeO_3$-type modifications to the perovskite structure are directly related to the octahedral rotation that is responsible

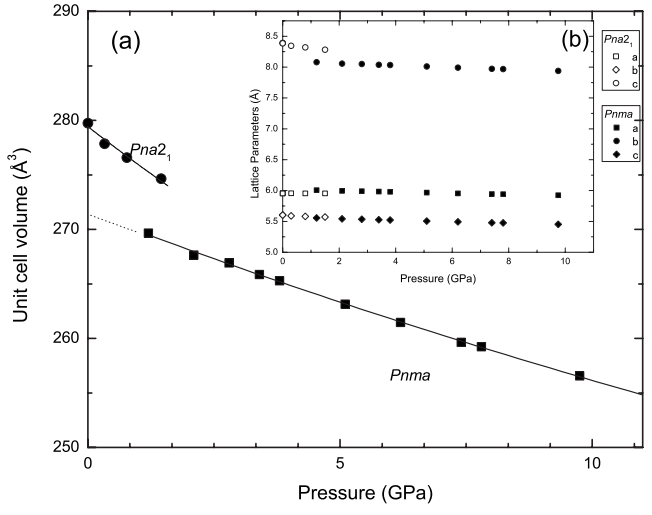

FIG. 13. X-ray profiles from $BiInO_3$ sample. History of pressure is indicated by the right axis. Monochromatic x-ray radiation of 38 keV was used.

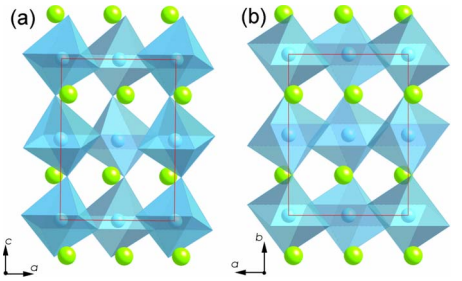

FIG. 14. (Color online) Schematic view of (a) $Pna2_1$ perovskite structure along the *b* axis and (b) *Pnma* perovskite structure along the *c* axis in $BiInO_3$. Large spheres and small spheres are bismuth and indium, respectively. Oxygen is not shown. Polyhedra indicate InO_6 octahedra.

for reducing the *A* site in the perovskite structure. According to the geometrical relationship,[28] the octahedral rotation (Φ) can be calculated from cell dimensions as follows:

$$\Phi = (\sqrt{2}c^2)/ab. \quad (1)$$

Namely, increasing Φ in $BiInO_3$ with pressure implies that the Bi site gradually shrinks to keep the structure (Fig. 15).

The Raman spectra show the difference between $Pna2_1$ and *Pnma* phases more clearly (Fig. 16). According to the factor group analysis,[33] 57 $(14A_1+15A_2+14B_1+14B_2,)$ modes are expected for the Raman active modes of $Pna2_1$. We experimentally observed 22 modes for the $Pna2_1$ phase.[9] While the analysis for the *Pnma* phase predicts 24 $(7A_g+5B_{1g}+7B_{2g}+5B_{3g})$ modes, we only observed 13 modes (Fig. 16). However, in the case of unpolarized measurements using a powdered sample, the number of the observed Raman modes in the *Pnma* perovskite is usually about twice smaller than the predicted number of 24, for example, 12 in $LaYbO_3$ (Ref. 41) and in $LaMnO_3$.[42] The same situation would be expected for $Pna2_1$ perovskite. Therefore, a reduction by half of the expected modes would be still reasonable for this high-pressure transition. Although we could not assign all of the Raman modes, two soft modes can be recognized at 148 and 360 cm^{-1}. The former mode completely vanishes after the transition. On the other hand, the latter mode remains but shifts toward higher wavenumber after the transition. Further investigations using *ab initio* calculations will be needed to make assignments for the Raman modes.

D. Systematic interpretation of Bi*M*O_3 (*M*=Al,Ga,In) perovskites

The present study revealed various unquenchable perovskite structures crystallizing under high pressure. Here, we give systematic interpretations for the perovskites in these compounds. The tolerance factor, *t*, indicating the geometrical allowance for cations to form perovskite structures in ABO_3 compounds is as follows:

$$t = (r_A + r_O)/\sqrt{2}(r_B + r_O), \quad (2)$$

where *r* denotes the ionic radii of each element.

According to Shannon (1976),[43] the *B* site cationic radii (r_B) for sixfold Al^{3+}, Ga^{3+}, and In^{3+} are 0.535 Å, 0.62 Å,

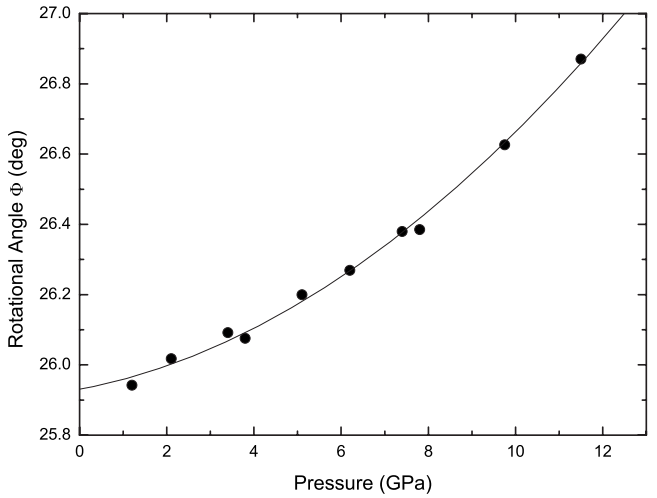

FIG. 15. Variation in rotational angle (Φ) of InO_6 octahedra with pressure.

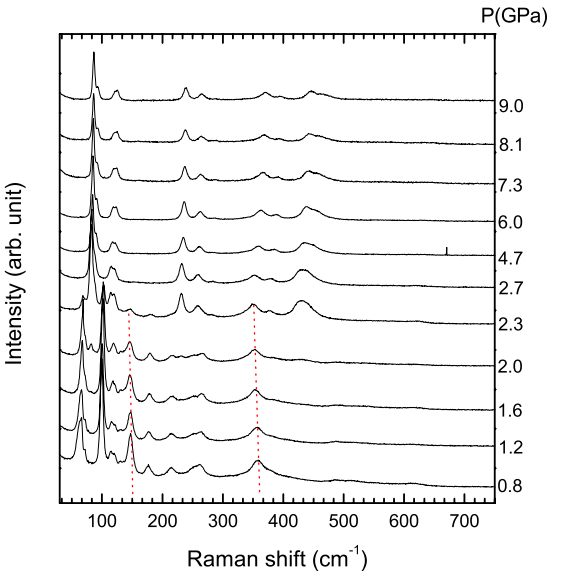

FIG. 16. (Color online) Variation in unpolarized Raman spectra from $BiInO_3$ samples with pressure under quasihydrostatic compression. Soft modes are shown by dotted lines.

and 0.80 Å, respectively, and the radius of O^{2-} (r_O) is 1.40 Å. However, there are no 12-fold cationic radii of Bi^{3+} in the table of this reference. We tried to estimate the cationic radii of Bi^{3+} from the ionic radii of Pb^{3+}, whose $6s^2$ electronic configuration is similar to that of Bi^{3+}. We increased the ionic radii of Bi^{3+} by 15% to 0.9 Å, as in Pb^{3+} from eightfold to 12-fold coordination. Using these ionic radii, t for $BiAlO_3$, $BiGaO_3$, and $BiInO_3$ perovskites are calculated to be 1.00, 0.96, and 0.88. In the case of perovskites with t being unity, the structure is close to ideal cubic perovskite. This t corresponds to that of $BiAlO_3$, rhombohedral perovskites with dodecahedral sites similar to cubic perovskite. If t is less than unity, the octahedral rotation settles the smaller cations into the A site. Thus, the small t of $BiInO_3$ is consistent with the appearance of $GdFeO_3$-type modifications. On the other hand, the smallest Al^{3+} prevents $BiAlO_3$ from transforming into a $GdFeO_3$-type modification up to 11 GPa. The tolerance factor does not reflect the displacement of the central atom in the octahedron. Therefore, the Cm phase would not be expected to crystallize in $BiGaO_3$. The stabilization of the pyroxene structure in $BiGaO_3$ could not be anticipated. The reason is that Ga^{3+} prefers fourfold oxygen coordination at lower pressure, as occurs in Ga_2O_3.[44]

Other than the present perovskites, the $GdFeO_3$ structure appears in Bi compounds under high pressure, such as $BiFeO_3$,[21] $BiScO_3$, $BiMnO_3$, and $BiCrO_3$.[18] This suggests that high-pressure synthesis plays an important role in producing solid-solution perovskites of these compounds. Even if different perovskite structures stabilize at ambient pressure, such as $Pna2_1$ in $BiInO_3$ and $R3c$ in $BiFeO_3$, it might be possible to synthesize $Bi(In,Fe)O_3$ solid-solutions under pressure, where $Pnma$ perovskites stabilize in each compound. Furthermore, if the structural relaxation to the noncentrosymmetric phase occurs during pressure release, the solid solutions would be a polar crystal at ambient pressure.

IV. SUMMARY

We have revealed the high-pressure phase transitions of $BiAlO_3$, $BiGaO_3$, and $BiInO_3$ by analyzing *in situ* x-ray diffraction and Raman scattering measurements. We confirmed that (1) AlO_6 octahedral rotation in the rhombohedral phase is responsible for the symmetry change from $R3c$ to $R3m$ in $BiAlO_3$, (2) the $BiGaO_3$ pyroxene phase transformed into a ferroelectric phase, as predicted by *ab initio* calculations, and (3) the noncentrosymmetric ($Pna2_1$) to centrosymmetric ($Pnma$) transition that occurs within $GdFeO_3$-type perovskite in $BiInO_3$.

ACKNOWLEDGMENTS

The synchrotron radiation experiments were conducted at BL-04B2 of SPring-8 with the approval of JASRI (Proposals No. 2006B1134, No. 2007B1192, and No. 2007B1147). H.Y. and A.A.B. acknowledge support from NIMS Competitive Research Fund. This work was partially supported by World Premier International Research Center Initiative (WPI Initiative, MEXT, Japan).

*yusa.hitoshi@nims.go.jp
†alexei.belik@nims.go.jp
‡muromachi.eiji@nims.go.jp
§hirao@spring8.or.jp
‖ohishi@spring8.or.jp

[1] J. Wang *et al.*, Science **299**, 1719 (2003).
[2] N. Hur, S. Park, P. A. Sharma, J. S. Ahn, S. Guha, and S.-W. Cheong, Nature (London) **429**, 392 (2004).

[3] P. Ravindran, R. Vidya, A. Kjekshus, H. Fjellvag, and O. Eriksson, Phys. Rev. B **74**, 224412 (2006).
[4] V. V. Shvartsman, W. Kleemann, R. Haumont, and J. Kreisel, Appl. Phys. Lett. **90**, 172115 (2007).
[5] D. Lebeugle, D. Colson, A. Forget, M. Viret, P. Bonville, J. F. Marucco, and S. Fusil, Phys. Rev. B **76**, 024116 (2007).
[6] P. Baettig, R. Seshadri, and N. A. Spaldin, J. Am. Chem. Soc. **129**, 9854 (2007).
[7] P. Baettig, C. Schelle, R. LeSar, U. Waghmare, and N. Spaldin, Chem. Mater. **17**, 1376 (2005).
[8] A. A. Belik, T. Wuernisha, T. Kamiyama, K. Mori, M. Maie, T. Nagai, Y. Matsui, and E. Takayama-Muromachi, Chem. Mater. **18**, 133 (2006).
[9] A. A. Belik, S. Y. Stefanovich, S. Y. Lazoryak, and E. Takayama-Muromachi, Chem. Mater. **18**, 1964 (2006).
[10] A. A. Belik *et al.*, J. Am. Chem. Soc. **128**, 706 (2006).
[11] H. Wang, B. Wang, R. Wang, and Q. Li, Physica B **390**, 96 (2007).
[12] H. Wang, B. Wang, Q. Li, Z. Zhu, R. Wang, and C. H. Woo, Phys. Rev. B **75**, 245209 (2007).
[13] C. Li, H. Wang, B. Wang, and R. Wang, Appl. Phys. Lett. **91**, 071902 (2007).
[14] P.-E. Janolin, P. Bouvier, J. Kreisel, P. A. Thomas, I. A. Kornev, L. Bellaiche, W. Crichton, M. Hanfland, and B. Dkhil, Phys. Rev. Lett. **101**, 237601 (2008).
[15] A. Sani, M. Hanfland, and D. Levy, J. Solid State Chem. **167**, 446 (2002).
[16] M. Ahart, M. Somayazulu, R. Cohen, P. Ganesh, P. Dera, H.-K. Mao, R. Hemley, Y. Ren, and P. Liermann, Nature (London) **451**, 545 (2008).
[17] M. Azuma, S. Carlsson, J. Rodgers, M. G. Tucker, M. Tsujimoto, S. Ishikawa, S. Isoda, Y. Shimakawa, and M. Takano, J. Am. Chem. Soc. **129**, 14433 (2007).
[18] A. Belik, H. Yusa, N. Hirao, Y. Ohishi, and E. Takayama-Muromachi, Inorg. Chem. **48**, 1000 (2009).
[19] R. Haumont, J. Kreisel, and P. Bouvier, Phase Transitions **79**, 1043 (2006).
[20] A. G. Gavriliuk, V. V. Struzhkin, I. S. Lyubutin, and I. A. Troyan, JETP Lett. **86**, 197 (2007).
[21] R. Haumont, P. Bouvier, A. Pashkin, K. Rabia, S. Frank, B. Dkhil, W. A. Crichton, C. A. Kuntscher, and J. Kreisel, Phys. Rev. B **79**, 184110 (2009).
[22] A. Belik, H. Yusa, N. Hirao, Y. Ohishi, and E. Takayama-Muromachi, Chem. Mater. **21**, 3400 (2009).
[23] P. M. B. H. K. Mao and J. Xu, J. Geophys. Res. **91**, 4673 (1986).
[24] A. P. Hammersley, European Synchrotron Radiation Facility Internal Report No. ESRF97HA02T, 1997 (unpublished).
[25] A. C. Larson and R. B. V. Dreele, Los Alamos National Laboratory Report LAUR, 2004 (unpublished), pp. 86–748.
[26] F. Izumi and T. Ikeda, Mater. Sci. Forum **321-324**, 198 (2000).
[27] H. Yusa, N. Sata, and Y. Ohishi, Am. Mineral. **92**, 648 (2007).
[28] R. H. Mitchell, *Perovskites: Modern and Ancient* (Almaz Press, Ontario, 2002).
[29] J. F. Scott, Phys. Rev. **183**, 823 (1969).
[30] M. V. Abrashev, A. P. Litvinchuk, M. N. Iliev, R. L. Meng, V. N. Popov, V. G. Ivanov, R. A. Chakalov, and C. Thomsen, Phys. Rev. B **59**, 4146 (1999).
[31] P. Bouvier and J. Kreisel, J. Phys.: Condens. Matter **14**, 3981 (2002).
[32] J. Zhao, N. L. Ross, and R. J. Angel, J. Phys.: Condens. Matter **16**, 8763 (2004).
[33] D. L. Rousseau, R. P. Bauman, and S. P. S. Porto, J. Raman Spectroscopy **10**, 253 (1981).
[34] G. H. Kwei, A. C. Lawson, S. J. L. Billinge, and S.-W. Cheong, J. Phys. Chem. **97**, 2368 (1993).
[35] A. A. Belik, M. Azuma, T. Saito, Y. Shimakawa, and M. Takano, Chem. Mater. **17**, 269 (2005).
[36] R. V. Shpanchenko, V. V. Chernaya, A. A. Tsirlin, P. S. Chizhov, D. E. Sklovsky, and E. V. Antipov, Chem. Mater. **16**, 3267 (2004).
[37] C. N. W. Darlington and K. S. Knight, Acta Crystallogr., Sect. B: Struct. Sci. **55**, 24 (1999).
[38] B. J. Kennedy, C. J. Howard, and B. C. Chakoumakos, Phys. Rev. B **60**, 2972 (1999).
[39] D. L. Corker, A. M. Glazer, J. Dec, K. Roleder, and R. W. Whatmore, Acta Crystallogr., Sect. B: Struct. Sci. **53**, 135 (1997).
[40] T. Hahn, *International Table for Crystallography*, 5th ed. (Kluwer, Dordrecht, 2002).
[41] R. L. Moreira, A. Feteira, and A. Dias, J. Phys.: Condens. Matter **17**, 2775 (2005).
[42] M. N. Iliev, M. V. Abrashev, H.-G. Lee, V. N. Popov, Y. Y. Sun, C. Thomsen, R. L. Meng, and C. W. Chu, Phys. Rev. B **57**, 2872 (1998).
[43] R. D. Shannon, Acta Crystallogr., Sect. A: Cryst. Phys., Diffr., Theor. Gen. Crystallogr. **32**, 751 (1976).
[44] H. Yusa, T. Tsuchiya, N. Sata, and Y. Ohishi, Phys. Rev. B **77**, 064107 (2008).